Journal of
Composites Science

MDPI

Article

Preparation, Characterization and Evaluation of Polyamide-Reduced Graphene Oxide as Selective Membranes for Water Purification

Ahmed A. Alshahrani [1], Abeer A. El-Habeeb [2,*], Arwa A. Almutairi [2], Dimah A. Almuaither [2], Sara A. Abudajeen [2], Hassan M. A. Hassan [3] and Ibrahim Hotan Alsohaimi [3,*]

[1] Nuclear Technologies Institute, King Abdul Aziz City for Science and Technology, P.O. Box 6086, Riyadh 11442, Saudi Arabia
[2] Department of Chemistry, College of Science, Princess Nourah Bint Abdulrahman University, P.O. Box 84428, Riyadh 11671, Saudi Arabia; almutiriarwa@gmail.com (A.A.A.); deemahabdulrahman@gmail.com (D.A.A.); saraabudajeen@gmail.com (S.A.A.)
[3] Chemistry Department, College of Science, Jouf University, P.O. Box 2014, Sakaka 72341, Saudi Arabia; hmahmed@ju.edu.sa
* Correspondence: aaalhabeeb@pnu.edu.sa (A.A.E.-H.); ehalshaimi@ju.edu.sa (I.H.A.)

Abstract: Amidst the ongoing advancements in membrane technology, a leading method has come to the forefront. Recent research has emphasized the substantial influence of surface attributes in augmenting the effectiveness of thin-film membranes in water treatments. These studies reveal how surface properties play a crucial role in optimizing the performance of these membranes, further establishing their prominence in the field of membrane technology. This recognition stems from the precise engineering of surfaces, ensuring they meet the demanding requirements of advanced separation processes. This study utilizes polyamide as a discerning layer, applied atop a polysulfone support sheet through interfacial polymerization (IP) for membrane fabrication. The amounts in the various membranes were created to vary. The membrane's permeability to water with significant salt rejection was enhanced, which improved its effectiveness. The polyamide (PA) membrane comprising graphene oxide (rGO, 0.015%) had a water permeability of 48.90 L/m^2 h at 22 bar, which was much higher than the mean permeability of polyamide membranes (25.0 L/m^2 h at 22 bar). On the other hand, the PA–rGO/CHIT membranes exhibited the lowest water permeability due to their decreased surface roughness. However, the membranes' effectiveness in rejecting salts ranged from 80% to 95% for PA–rGO and PA–rGO/CHIT membranes.

Keywords: membranes; polyamide; chitosan; reduced graphene oxide; salt rejection

Citation: Alshahrani, A.A.; El-Habeeb, A.A.; Almutairi, A.A.; Almuaither, D.A.; Abudajeen, S.A.; Hassan, H.M.A.; Alsohaimi, I.H. Preparation, Characterization and Evaluation of Polyamide-Reduced Graphene Oxide as Selective Membranes for Water Purification. *J. Compos. Sci.* **2024**, *8*, 24. https://doi.org/10.3390/jcs8010024

Academic Editors: Francesco Tornabene, Niranjan Patra and Sayan Ganguly

Received: 30 November 2023
Revised: 25 December 2023
Accepted: 8 January 2024
Published: 10 January 2024

1. Introduction

As population increases and industry advances, access to clean, potable water is an urgent problem [1,2]. The cost-effective process for producing fresh water from seawater is reverse osmosis membrane [3]. Among membrane technologies, reverse osmosis is the most widely employed technique, particularly for those that use semi-permeable membranes to extract solutes from water. High hydraulic pressure is used in reverse osmosis (RO) to offset the osmotic pressure found in water [4,5]. The tiny holes of semi-permeable membranes allow H_2O to pass through freely, but they block solutes that are restricted to the membrane's pressured side from doing so. Brine, or concentrated saline solution, and filtered water are the products of the process. Commercial systems usually reach a recovery rate (given as a percentage) higher than 60%, which is determined by dividing the final desalinated water volume by the original water input [4,6]. The field of nanofiltration membrane technology has come a long way since its inception in the late 1980s [7]. Nanofiltration (NF) membranes are positioned between reverse osmosis and ultrafiltration (UF). They usually have a pore size of around 1 nm, which corresponds

to a molecular weight cut-off (MWCO) of 300–500 Da. Because of the adsorption of charged solutes or the dissociation of surface functional moieties, NF membranes display a modest charge when in contact with an aqueous solution. In the presence of a feed solution, polymeric NF membranes, for instance, have a charged surface because they include ionizable groups like carboxylic and sulfonic acid groups [7]. NF membranes are effective in separating inorganic ions and small organic molecules; they resemble RO membranes. Low rejection of monovalent ions, strong rejection of divalent ions, and greater flow in comparison to RO membranes are the main features that set NF membranes apart from RO membranes. Polyamide (PA) selective layers are applied on porous substrates to develop most commercial membranes [8]. A typical interfacial polymerization procedure involves submerging porous substrates (particularly sheets of polysulfone), soaked in m-phenylenediamine (MPD) solution, in water and trimethyl chloride (TMC) solution, to fabricate PA-selective layers of RO membranes for salt rejection [9,10]. Although PA membranes outperform the initial cellulose acetate membranes regarding transmission and salt rejection, there is a pressing need for advancements in practical applications. Balancing water permeability and salt rejection remains challenging, emphasizing the ongoing focus on developing membranes to overcome this trade-off. This remains a central area of study in membrane technology [11–13].

Graphene oxide (GO) is a potential material for PA membranes for desalination. A strongly oxidized version of graphene, called graphene oxide, has oxygen-containing moieties comprising hydroxyl, carboxylic acid and epoxide [14,15]. Functional moieties make hydrophilicity possible by allowing GO flakes to scatter in water and permitting a variety of water purification techniques [16]. Composite graphene membranes are studied using various materials like graphene oxide, powder, and polymeric nanofibers. Positioning and orientation are influenced by the process, with high GO orientation achieved through pressure-assisted techniques or spin coatings. Membranes require metallic, ceramic, or polymeric scaffoldings for forward or reverse osmosis [17–20]. Researchers developed nanomaterial-based thin films on various substrates, including flexible touch screens, barrier films, transparent electrodes, and graphene oxide membranes using rod coating [21]. Via the use of interfacial polymerization (IP), inorganic nanoparticles, which include titanium dioxide [22], zeolites [23,24], functionalized carbon nanotubes [25,26], silicon dioxide [27], GO, and rGO [24] are added to the polyamide (PA) matrix. Thin-film nano-composite (TFN) membranes are created by dispersing nanoparticles in aqueous or organic phases to increase chlorine resistance, fouling, and water transport. The development of high-quality RO membranes depends on discovering innovative, efficient nanoparticles with tiny sizes and evenly distributed precursor solutions. Research demonstrates that GO nanoparticles enhance chlorine resistance, water flow and antifouling and antibacterial properties [28–30]. GO flakes improve the organic separation's water flow and organic fouling resistance. In addition, GO flakes enhance anti-bacterial capabilities by reducing cell attachment. To enhance the efficacy of desalination, PA membranes are better suited to GO with smaller diameters [31,32]. The anti-fouling and chlorine resistance of the PA–TFN membranes were created by covalent bonds between PA and GO [31]. According to Choi et al., layer-by-layer deposition improved anti-fouling characteristics by 56% and boosted water flow by 12% [12]. For TFN membranes containing GO, Ali et al. [33], Chae et al. [34] and Kim et al. [35]. showed increases in the water flow of 39%, 80% and 18%, respectively. The enhanced water flow brought on by these membranes' nano-channels and surface hydrophilicity allowed them to demonstrate superior resistance to chlorine attack and fouling. Hydrophilic and negatively charged surfaces, which reduced foulant adhesion and facilitated foulant removal, were the cause of the improved antifouling property. The replacement of the chlorine is prevented by hydrogen bonding between GO and PA.

Graphene oxide (GO) and its components have found extensive applications as fillers in the creation of separation membranes for both gas [36,37] and liquid [31,38] phases. In liquid phase applications, thin film nanocomposite (TFN) membranes incorporating graphene derivatives have predominantly been utilized in aqueous processes like nanofiltration

(NF) and pervaporation (PV). Chae et al. [31] employed GO as a filler in the fabrication of TFN membranes, resulting in membranes with improved antifouling features and greater water fluxes in RO. Similar outcomes, coupled with enhanced chlorine resistance, were observed by Song et al. [13] using GO quantum dots as fillers. Wang et al. [39] incorporated ZIF-8 (zeolitic imidazolate framework-8)/GO hybrid nanosheets as fillers in the production of antimicrobial TFN membranes, displaying significant antimicrobial performance improvement. Ma et al. [40] fabricated TFN membranes by functionalizing GO with poly(sulfobetaine methacrylate) and utilized them in nanofiltration, leading to an increased water flux, as well as improvements in antimicrobial performance and antifouling characteristics, compared to thin film composite (TFC) membranes. Xue et al. [41] enhanced the flux and chlorine resistance of TFC membranes in salt nanofiltration by employing GO as a filler in the fabrication of TFN membranes. A recent study by Alberto et al. [42] addressed this gap, developing TFN membranes for n-butanol/water separation through pervaporation. They embedded GO derivatives into a high free-volume thin film polymer framework, resulting in an improved separation efficiency compared to bare TFC membranes. Therefore, despite the widespread use of graphene-based fillers in TFN membranes for aqueous applications, there is limited research on graphene as fillers and their application in RO membranes for desalination activities.

This paper details the synthesis of polyamide (PA)-based membranes, which incorporate reduced graphene oxide (rGO) nanoparticles. An additional innovation lies in using these membranes in water desalination activities. The decoration of rGO with PA creates hydrophilic graphene-based nanofillers, which exhibit improved dispersion in the organic phase during interfacial polymerization (IP). The study evaluated the activity of these RO membranes in NaCl salt separation.

2. Experimental

2.1. Materials

Chitosan (medium molecular weight) was used as a surfactant when reducing the graphene oxide and was purchased from Sigma-Aldrich (St. Louis, MO, USA) at a concentration of 0.1% (w/v). Reduced graphene oxide (rGO), which is used as a unique material that is treated to reduce the oxygen bonds, was provided by Graphene Chemical Industries (Ankara, Turkey). The PS-20 Polysulfone Membrane Sheet was purchased from Sepro in Oceanside, CA, USA. Both 1,3,5-benzenetricarbonyl trichloride ($C_9H_3Cl_3O_3$, 98%) and 1,3-phenylenediamine ($C_6H_8N_2$, 99.5%) were bought from Kenilworth, New Jersey, NJ, USA. Hexane (C_6H_{14}, 99%) was acquired from Oxford Laboratory in Mumbai, India. The sodium chloride (NaCl, 99%) was given by Sigma-Aldrich Chemicals in Hamburg, Germany. The 100% ethanol that was acquired was provided by Finechem Pty, Ltd. of South Wales, Australia. In this study, Milli-Q® water (Millipore Corporation, Bedford, TX, USA) (resistivity 18.2 MΩ·cm) was utilized to create both solutions and dilutions.

2.2. Materials Fabrication

2.2.1. Preparation of Polyamide (PA) Membrane

Commercial polysulfone protection sheets are dipped in distilled water for 24 h to remove the lipid layer. Membranes made of polyamide (PA) can be created by extending the selective PA layer downward. The development of the composite membranes involved applying an interfacial polymerization (IP) reaction between trimesoyl chloride (TMC) in organic solvents and meta-phenylene diamine (MPD) in an aqueous solution onto a polyethersulfone (PES) microporous substrate. The membrane' surface area measured 40 cm^2.

2.2.2. Preparation of Reduced Graphene Oxide (rGO) Membranes

The substrate (polyethersulfone sheets) was submerged in a reduced graphene oxide (rGO) solution at three different concentrations (0.005%, 0.01% and 0.015%, w/v), and the resulting membranes were then submerged in meta-phenylene diamine (MPD) solution

for two minutes, followed by submersion in 1,3,5-benzenetricarbonyl trichloride solution (0.1% w/v) for one minute, as shown in Figure 1.

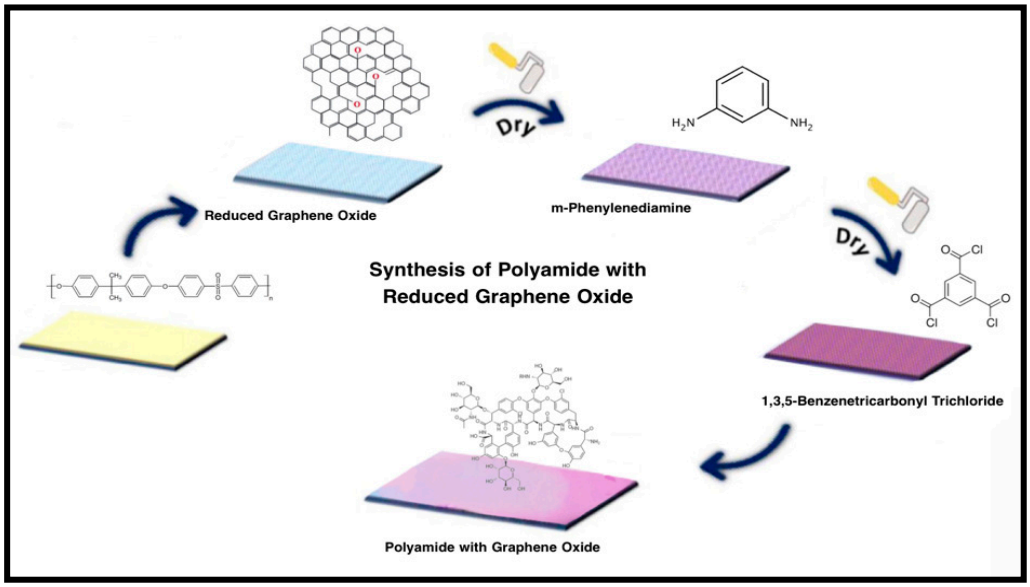

Figure 1. Synthesis of PA–rGO (0.005%, 0.01% and 0.015% w/v) membranes.

2.2.3. Fabrication of Chitosan (CHIT)–Reduced Graphene Oxide (rGO) Membranes

Chitosan (CHIT) solution, provided as the rGO's solvent, was dispersed with three different concentrations of reduced graphene oxide (rGO): 0.005%, 0.01% and 0.015%, w/v. Following the coating of the polyethersulfone sheets with CHIT/rGO solutions, they were allowed to dry for an hour at 50 C. The resulting membranes then undertook a two-minute soak in m-phenylenediamine (MPD, 2% w/v) solution and a one-minute soak in 1,3,5-benzenetricarbonyl trichloride solution (0.1 w/v), as shown in Figure 2.

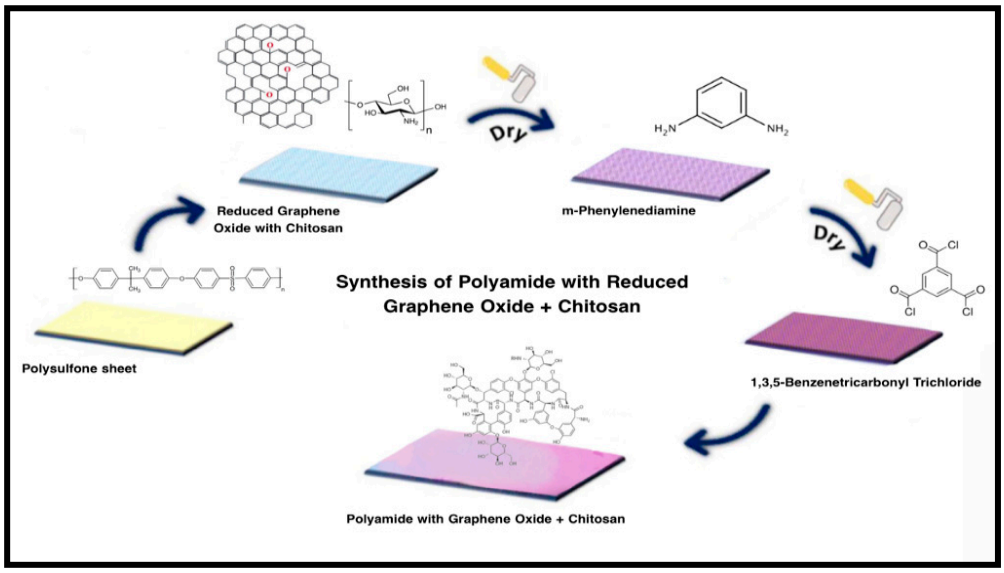

Figure 2. PS–PA–rGO–CHIT (0.005%, 0.01% and 0.015% w/v) membrane.

2.3. Characterization

Fourier Transform Infrared (FTIR) spectroscopy was utilized to investigate the structures of the fabricated membranes. Field emission scanning electron microscope (FESEM) was employed to examine surface morphologies and cross areas of layers, coated twice

with a JEOL JEC 3000FC fine coater, and examined at varying amplification voltages. A PerkinElmer analyzer performed thermogravimetric analysis (TGA) on membranes, using nitrogen gas and a heating rate of 10 °C/min. We measured the contact angles of water (4 µL) on the membrane surface using a SCA20 goniometer, averaging ten droplets. The SurPASS electrokinetic analyzer measured membrane zeta potentials using a (1) mM KCl electrolyte solution, with pH values between 2.5 and 5.5 obtained for automated titration measurements.

2.4. Salt Rejection Performance

The investigation of RO membranes involved conducting water permeability and salt rejection measurements using a laboratory-scale crossflow NF/RO system. Milli-Q® water was uniformly applied to all membranes under a pressure of 25 bar to compact them prior to the filtration experiments. The membrane compression process lasted from nearly 30 min to 1 h, continuing until a stable baseline flux was achieved. Following membrane compaction, the permeate flux of DI water was assessed at various applied pressures to determine the water permeability of the membranes. At room temperature, Milli-Q® water was utilized in each experiment, and Equation (1) was employed to calculate the water flow.

$$J = V/A \times t \quad (1)$$

where J is the water flow (L/m^2 h), A is the membrane area (m^2), V is the permeation volume (L), t is the treatment duration (h) and V is the volume of permeation (L).

To evaluate salt rejection, individual salt solutions (NaCl) at a concentration of 2 g/L were utilized. The crossflow velocity was set at 34.7 cm/s, equivalent to a cross flow of 100 L/h. Throughout the experiment, the temperature of the feed solution was consistently maintained at 20 ± 2 °C with the assistance of a chiller. Equation (2) was used for determining the salt rejection (R):

$$R\% = (1 - C_P/C_f) \times 100 \quad (2)$$

where C_p and C_f are, respectively, the permeate and feed streams' salt concentrations.

3. Results and Discussion

The features of the composite material can alter significantly when modified graphene oxide (GO) is added to polyamide (PA). Reduced graphene oxide (rGO) is a graphene derivative composed of graphene sheets with functional moieties, including carboxyl, epoxy and hydroxyl groups including oxygen. To increase graphene oxide's compatibility with the polyamide matrix and the composite material's overall performance, different functional groups or chemical moieties are introduced into the rGO. Because of its high aspect ratio and two-dimensional structure, modified graphene oxide can be a reinforcing filler in the polyamide matrix. Strong covalent bonds between the polyamide chains and the functionalized graphene oxide provide this reinforcement. The thermal conductivity of a graphene derivative is outstanding, and the polyamide composite's thermal conductivity may be increased by adding modified rGO. This improvement is essential for applications like electrical devices, where heat dissipation is critical. The polyamide matrix's enhanced thermal resilience can be assigned to the modified GO, which lowers the risk of thermal deterioration at high temperatures. An improved load transfer and overall mechanical performance can result from chemical changes to the graphene oxide surface, which can also increase interfacial adhesion with the polyamide matrix.

In order to synthesize graphene oxide (GO) and its derivatives' suspensions, reduced graphite oxide (rGO) was synthesized using a modified Hummers technique [43,44]. The microfilmer paper was soaked in an aqueous MPD solution containing rGO nanoparticles to create PA–rGO and PA–rGO/CHIT membranes, which were then polymerized in a TMC n-hexane solution. The electrostatic contact causes the MPD particles to become trapped with GO in membranes. Additionally, a reaction between the MPD amino groups and oxygen-

containing rGO develops [45]. In rGO nanoparticles, oxygen-containing groups provide negatively charged edges, which reduce permeability with higher loading and enable efficient polymerization control through specified interfaces [46]. To manage nanochannel size and enhance salt rejection, PA preferentially develops on rGO edges and flaws. It does this by adsorbing more MPD molecules that contain amino groups.

3.1. Morphology of Membranes

The substrate, the PA–rGO membranes with rGO loading of 0.005, 0.01, and 0.015 w/v, and the PA–rGO/CHIT membrane are all shown in SEM images in Figure 3A–F. It was clear that substrates were coated in a continuous PA–rGO layer, and surface images demonstrate that the rGO nanoparticles change the shape of the PA membrane, as shown in Figure 3A–D. The surface of the membrane exhibits a characteristic "ring-like" morphology, confirming the accurate synthesis of the PA thin layer. Moreover, no visible aggregates are observed, indicating effective filler (rGO) dispersion during the thin PA layer synthesis [47,48]. According to studies, surface roughness in IP reactions is increased by nanoparticles such as zeolite, CNT, TiO_2, SiO_2 and GO [49–52]. Conversely, the SEM images distinctly reveal that the critical factor influencing surface alterations in Figure 3E,F is the introduction of chitosan, which serves as a substance facilitating the dispersion of reduced graphene oxide (rGO) throughout the membrane surface. These observations are consistent with previous research utilizing chitosan as a dispersing agent [53,54]. This is ascribed to chitosan enveloping nanoparticles, aiding in dispersion, and concurrently offering comprehensive coverage, leading to a decrease in surface porosity. The PA–rGO membranes (Figure 3B–D) displayed more wrinkling and a darker brown color following limited interfacial polymerization, compared to the PA–rGO/CHIT membranes (Figure 3E,F). As anticipated, the PA (Figure 3A) and PA–rGO (Figure 3B–D) membranes did not exhibit a leaf-like structure, in contrast to the membranes generated by PA–rGO/CHIT (Figure 3E,F). In comparison to the PA and PA–rGO membranes (Figure 3A–D), the PA–rGO/CHIT (Figure 3E,F) membranes were a little bit thicker (Figure 3D). It is clear from the images (Figure 3A–F) that PA–rGO/CHIT membranes mainly demonstrate that modifying the nanochannel size will have a more significant effect on increasing salt rejection than other membranes.

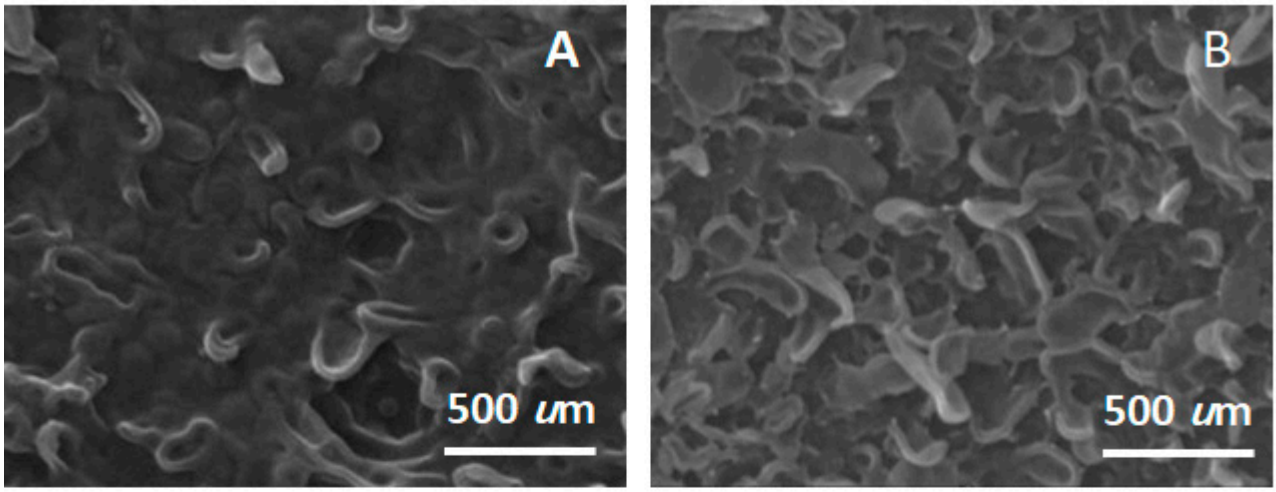

Figure 3. *Cont.*

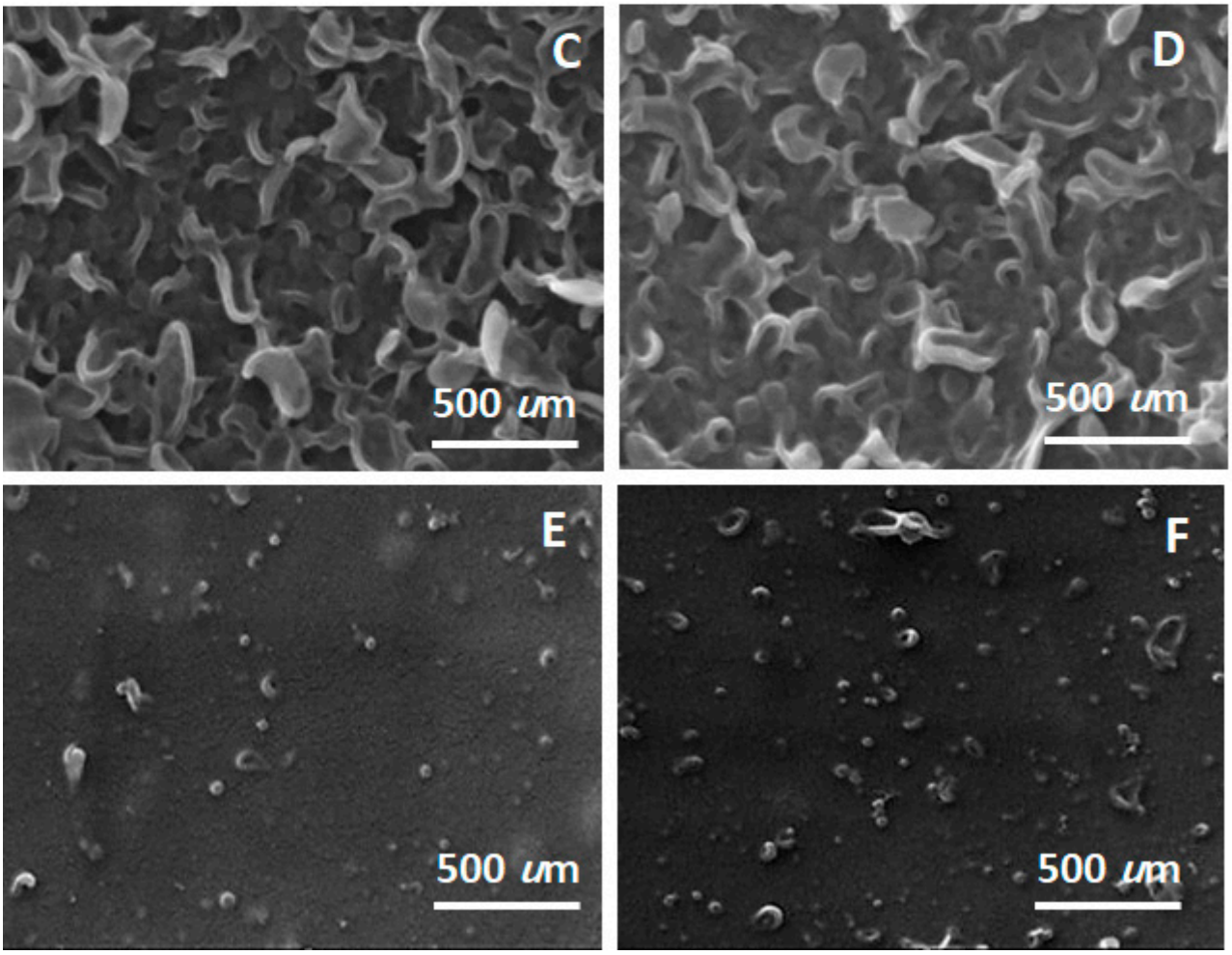

Figure 3. SEM images of (**A**) PA, (**B**) PA–rGO (0.005), (**C**) PA–rGO (0.01), (**D**) PA–rGO (0.015), (**E**) PA–rGO (0.005)/CHIT and (**F**) PA–rGO (0.01)/CHIT membranes.

3.2. Contact Angle of Membranes

Semi-hydrophilic membranes have a contact angle of less than 90°, and as the angle drops, they become more effective at preventing fouling and influencing membrane flow [26,55]. The contact angle measures how a liquid behaves when it comes into contact with a membrane surface. It is often used to assess the wettability of a material and can provide insights into surface properties. The provided data appear to represent contact angle results for different types of membranes, as shown in Table 1. The PA (polyamide) membrane (38.2° ± 1.2°) has a relatively low contact angle. A lower contact angle indicates better wetting properties, meaning the liquid will likely spread more easily on the surface. The contact angle of the PA–rGO (0.005) membrane (47.2° ± 4.9°) increases, in comparison to pure polyamide. This could indicate a change in the surface properties, possibly due to the incorporation of the reduced graphene oxide (rGO). An increased contact angle might suggest decreased wettability. For the PA–rGO (0.01) membrane (58.1 ± 1.5), the contact angle increases further, indicating that the surface is becoming less wettable. The concentration of rGO seems to affect the surface properties of the membrane. For the PA–rGO (0.015) (49.62 ± 4.7) membrane, the value is lower than that of PA–rGO (0.01), but higher than that of PA–rGO (0.005). The concentration of rGO appears to have a complex effect on the contact angle, possibly indicating an optimal concentration for wettability. The hydrophilic character of the membrane is related to the existence of oxygen-containing functional moieties on the rGO sheets, where H-bonds may form between water molecules and oxygen atoms that are somewhat negatively charged, creating a very hydrophilic

surface [56]. For the PA–rGO (0.005)/CHIT membrane (42.25 ± 2.0), introducing chitosan (CHIT) seems to have decreased the contact angle, compared to PA–rGO (0.005) alone. CHIT may be contributing to improved wetting properties. The contact angle increases with the PA–rGO (0.01)/CHIT membrane (48.77 ± 1.1), compared to PA–rGO (0.005)/CHIT. The combination of rGO and CHIT might have a different impact on surface properties than each material alone. For the PA–rGO (0.015)/CHIT membrane (45.63 ± 4.1), the contact angle is between the values for PA–rGO (0.005)/CHIT and PA–rGO (0.01)/CHIT. The concentration of rGO and CHIT may interact in a way that affects the surface properties. The contact angle results suggest that adding rGO and CHIT can influence the wetting properties of the polyamide membranes. The concentration of these additives appears to play a role in measuring the contact angle, and the interactions between different materials can be complex. These results have implications for designing and optimizing membranes for specific applications, particularly those related to fluid interactions.

Table 1. The contact angle and water permeability of all membranes.

Membranes	Contact Angle	Water Permeability
	(°)	(L m^{-2} h^{-1} Bar^{-1})
PA	38.2 ± 1.2	1.05 ± 0.06
PA–rGO (0.005)	47.2 ± 4.9	2.05 ± 0.1
PA–rGO (0.01)	58.1 ± 1.5	1.52 ± 0.16
PA–rGO (0.015)	49.62 ± 4.7	2.00 ± 0.14
PA–rGO (0.005)/CHIT	42.25 ± 2.0	0.42 ± 0.04
PA–rGO (0.01)/CHIT	48.77 ± 1.1	0.86 ± 0.07
PA–rGO (0.015)/CHIT	45.63 ± 4.1	-

3.3. Fourier Transform Infrared Spectra of the Fabricated Membranes

The FTIR spectra are depicted in Figure 4. The polysulfone causes the peak values at 1488 and 1245 cm^{-1} (PS) to support C-O-C and CH3-C-CH3 stretching, respectively (Figure 4a). As per the FTIR spectra of the PA membrane (Figure 4a), the absorption peaks observed at 1151 cm^{-1} (indicating stretching of O-S-O), 1244 cm^{-1} (associated with stretching of C-O-C) and 1585 cm^{-1} (representing C-C aromatic modes) are indicative of the presence of sulfone groups. Additionally, the absorption at 1020 cm^{-1} and 830 cm^{-1} are due to the aromatic polysulfone ring's C-H stretching. The creation of the polyamide layer atop the polysulfone layer is supported by the FTIR spectra of the PA membrane (Figure 4b) and the absorbances at 1645 cm^{-1}, 1546 cm^{-1}, 1594 cm^{-1}, 1095–1020 cm^{-1} and 745–750 cm^{-1} in the spectra of PA membrane. The stretching of the amide linkage at the wavelengths of 1645 cm^{-1}, 1546 cm^{-1} and 1594 cm^{-1}, the bending of the amide bond at wavelengths of 1095 cm^{-1} and 1020 cm^{-1} and the stretching of the amide at wavelengths of 745–750 cm^{-1} are all related to the absorbance. After coating with rGO, the rGO membrane's FTIR spectrum (Figure 4c) revealed multiple prominent peaks, which indicated the presence of several chemical moieties, after anchoring the rGO membrane to a PA–PS substrate. The FTIR spectrum (Figure 4d) of the O-H moieties are located at 3350 cm^{-1}, the C=O from the carbonyl and carboxyl moieties are located at 1700 cm^{-1}, the sp^2 hybridized C=C is located at 1600 cm^{-1}, the C-O-C from the epoxy/ether moieties are located at 1200 cm^{-1} and the C-O related to alkoxy/alkoxide is located at 1037 cm^{-1} [56,57].

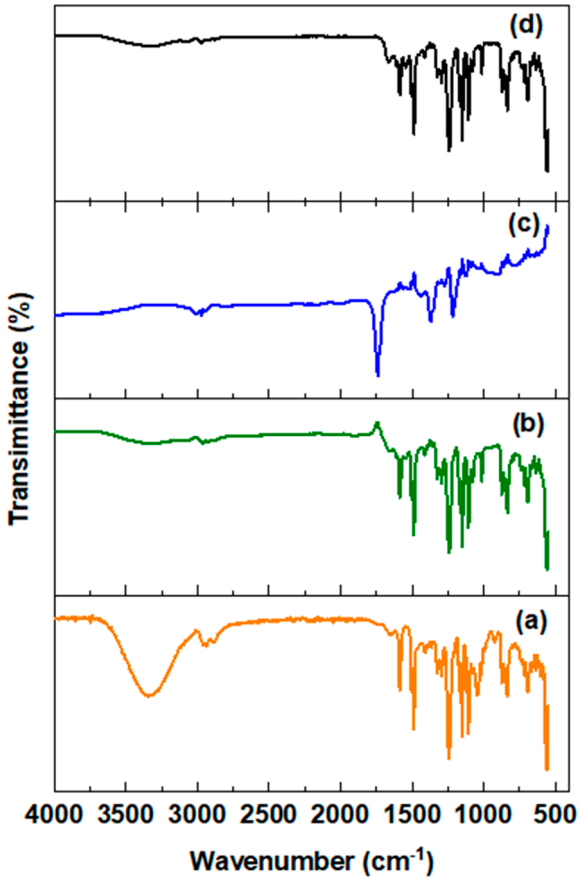

Figure 4. FTIR spectra of (**a**) polysulfone (PS), (**b**) polyamide, (**c**) PA–rGO and (**d**) PA–rGO/CHIT membranes with reduced graphene oxide (rGO) loading of 0.005, 0.01 and 0.15 *w*/*v*.

3.4. Thermogravimetric Analysis of Membranes

As illustrated in Figure 5, TGA tests were carried out to determine how rGO affected PA's thermal stability. At temperatures beginning at 440 °C, a weight loss for PA and PA–rGO membranes was observed (Figure 5A), which can be attributed to the breakdown of the PA polymer. All membranes' TGA curves showed that degradation began about at 440 °C and had a reasonably modest, progressively declining rate across a broad temperature range up to 721 °C. As amine and hydroxyl functional groups on PA–rGO are a little more sensitive to heat than those on PA [58], they can be taken off the top layer of PA–rGO. The breakdown of PA and PA–rGO/CHIT membranes (Figure 5B) began at a temperature that was similar to that of PA and PA–rGO membranes (Figure 5A), and only one significant mass loss can be detected beginning at 430 °C, following a similar pattern as the subsequent major weight loss of PA. The thermal stability of the PA membranes appears unaffected by the addition of rGO. This may be due to rGO's involvement in polymerization, which results in a more effectively cross-linked PA framework. The PA–rGO/CHIT membranes exhibited a slightly accelerated degradation, compared to both PA and PA–rGO membranes, particularly during the second significant mass loss phase. This implies that an excessive addition of CHIT to the top layer of PA could potentially lead to a decrease in the membranes' overall thermal stability.

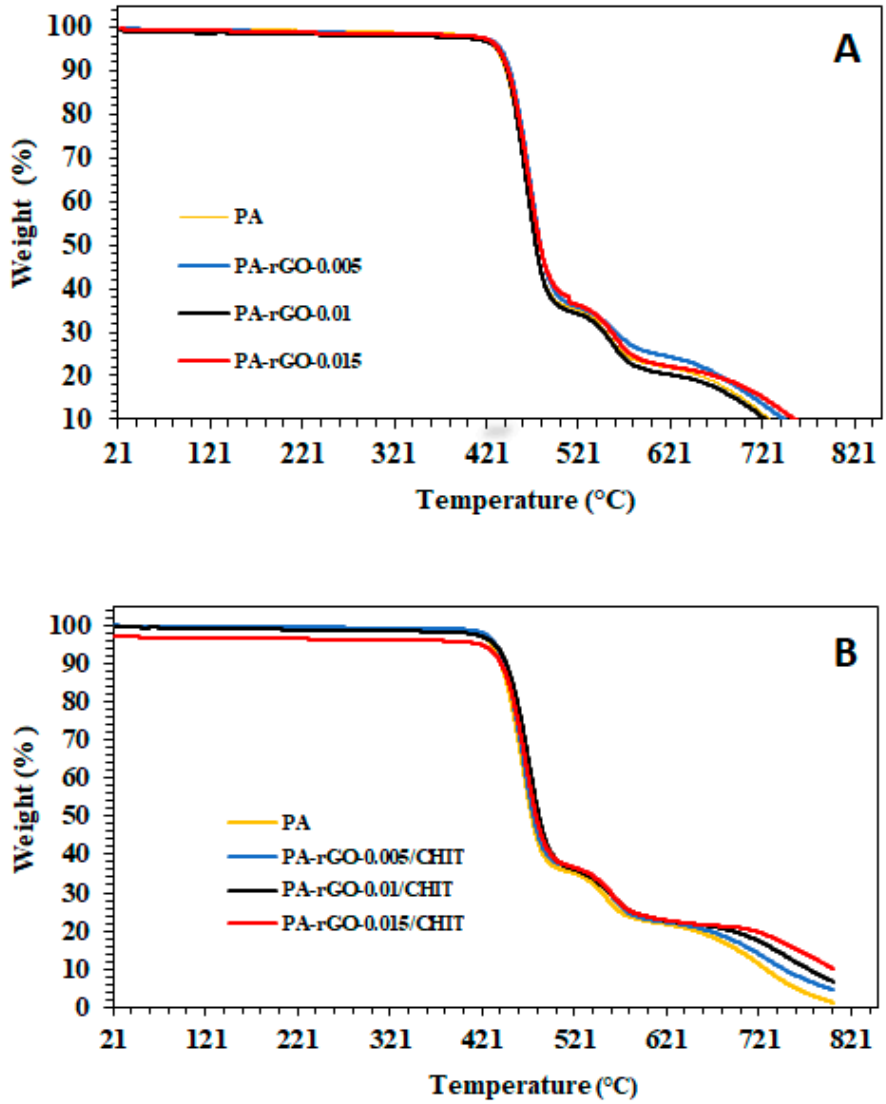

Figure 5. TGA results of (**A**) PA, PA–rGO (0.005), PA–rGO (0.01) and PA–rGO (0.015); (**B**) PA, PA–rGO (0.005)/CHIT, PA–rGO (0.01)/CHIT and PA–rGO (0.015)/CHIT membranes.

3.5. Water Permeability

The contact between the membrane surface and solution is altered by the surface charge, chemical make-up of the membrane and the hydrophilicity, which substantially affect the water flow rate. Additionally, columbic interaction and hydrogen bonding are only a few examples of the secondary forces that might mediate this interaction [26,59]. The permeate flux was drawn against the worked pressure for PA, PA–rGO (0.005%, 0.01% and 0.015% *w*/*v*) and PA–rGO–CHIT (0.005%, 0.01% and 0.015% *w*/*v*), respectively (Figure 6A–C) (Table 1). It is clear that, as expected, the flow across the membrane rises linearly with the introduced pressure variation. The permeability data were determined by calculating the regression slope between flow and worked pressure. The findings indicated that the water flux of the RO membrane for the PA–rGO (0.005% *w*/*v*) membrane increased by approximately 100%, compared to the PA membrane (20.00 L/m^2 h) at 18 bar pressures. The performance of the membrane is not significantly impacted by an increase in rGO concentration. The findings indicated that the PA–rGO membranes' RO membrane water flow was greater to that of the PA–rGO/CHIT membranes. The rGO/CHIT membrane's internal coating structure, which has a significant impact on the water transportation channel, may help explain this. Typically, water molecules traverse the inner layers of the GO laminates via the interlayer distance, after entering through the surface pores (flake-

to-flake lateral distance) on the membrane. This implies that the addition of extra layers, such as rGO and CHIT, elongates the path of water molecules. Consequently, this reduces water flux, a phenomenon in agreement with existing literature [56,60]. Furthermore, a positive intercept in the relationship between water flux and pressure, (Figure 6A–C) (Table 1), suggests that factors beyond the applied pressure contribute to the observed flux. Normally, one would anticipate a linear or proportional increase in water flux with pressure. However, the positive intercept implies additional complexities in the system. The existence of osmotic pressure in the feed salt solution introduces another layer of complexity to this relationship. Osmotic pressure typically opposes the flow of water across a membrane, counteracting the applied pressure. Additionally, the characteristics of the membrane, such as pore size, charge, or composition, could influence the intercept. Some membranes may display non-linear behavior, due to specific characteristics affecting water transport. Furthermore, temperature variations can impact the system's fluid dynamics, potentially causing deviations from the expected linear relationships.

3.6. Salt Rejection of Membranes

A cross-flow RO/NF system was used to assess each produced membrane's capacity to reject salt. Figure 7A–C show the salt rejection (NaCl) of the produced membranes using PA, PA–rGO (0.005%, 0.01% and 0.015%), and PA–rGO/CHIT (0.005% and 0.01%). NaCl, at a concentration of 2 g/L, was the salt that is rejected. In general, the membranes exhibit a rejection ratio ranging from 88% to 98%, indicating the potential for higher efficiency in the prepared membranes. The amount of NaCl that PA–rGO (0.005% w/v) (Figure 7A) rejects is rising. With a rise in the negative surface charge of the rGO blended membranes, salt rejections may be improved. The presence of several negatively charged groups in rGO is known to raise the repulsion between anions and the membrane surface [61]. Moreover, the salt rejection exhibits a slight increase with the rise in rGO concentration from 0.005% to 0.01% w/v, followed by a decline as the concentration of rGO reaches 0.015% w/v (Figure 7B). This pattern can be attributed to the accumulation of rGO on the membrane surface, leading to a diminished impact of graphene oxide (GO) functional groups. In connection with the aforementioned, the introduction of PA–rGO/CHIT (Figure 6C) has been proven to be an effective strategy to significantly enhance the PA membrane's surface hydrophilicity and create sparse large interfacial holes, thereby facilitating water transport. The optimization of PA–rGO/CHIT loading in the PA matrix at concentrations of 0.005% and 0.01% w/v demonstrates a substantial improvement in salt rejection (NaCl). In this work, PA–rGO membranes are compared to PA–rGO/CHIT membranes; the comparison shows that PA–rGO/CHIT membranes containing CHIT have greater NaCl rejection (95%), which closely resembles those of the PA membrane. As a result, rGO with CHIT may be a potential addition to developing high-rejection PA membranes for desalination. Table 2 lists the typical performance characteristics of the PA/reduced graphene oxide (rGO) membranes and other membranes reported in the literature [26,62]. The values of the water flow vary greatly between various membranes. PA–rGO (0.01)/CHIT has the lowest water flow (9.00 L/m^2 h^{-1}), whereas PA–SiO_2 (1%) has the greatest (47.9 L/m^2 h^{-1}). Moreover, PA–SiO_2 (1%) exhibits the maximum salt rejection (98.9%), whereas PA–rGO (0.01)/CHIT has the lowest (88.58%) salt rejection. The addition of several additives, including silica (SiO_2), chitosan (CHIT), reduced graphene oxide (rGO) and multi-walled carbon nanotubes (MWCNTs), has a discernible effect on salt rejection and water flow. Salt rejection and water flux appear to be mutually exclusive. Salt rejection is frequently correlated with higher water flow and vice versa. Membranes for salt rejection and low water flow, such as PA–rGO (0.01)/CHIT, clearly demonstrate this trade-off. The type of membrane to choose depends on the application's particular needs. Whether the desired process is desalination, water purification, or something else entirely, engineers and researchers have to weigh the trade-offs between water flux and salt rejection when choosing a membrane. The study assesses polyamide membranes in various desalination scenarios, including seawater reverse osmosis (SWRO), brackish water reverse osmosis (BWRO) and NF, focusing on

upper limits. SWRO membranes consistently achieve rejections exceeding 99%, while NF membranes display rejections below 90%. In desalination applications, PA, BWRO and SWRO membranes show significant rejection rates (Table 2), while PA–rGO and PA–rGO/CHIT membranes exhibit marginal reductions, striking a balance between advanced materials and rejection performance [63]. Despite unique properties, NF membranes have lower rejection rates, suitable for applications where some solute transit is acceptable. Overall, our findings highlight diverse membrane designs and rejection performances, aiding in selecting membranes for specific desalination or separation needs.

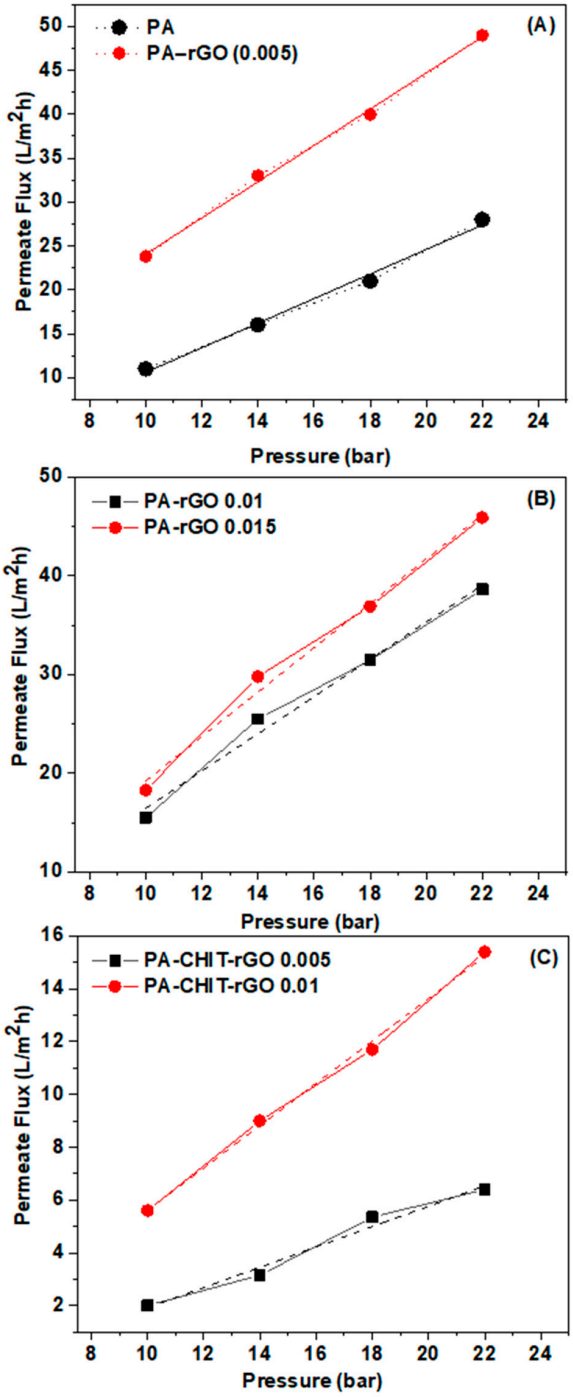

Figure 6. Water permeability of (**A**) PA and PA–rGO (0.005), (**B**) PA–rGO (0.01) and PA–rGO (0.015) and (**C**) PA–CHIT-rGO (0.005) and PA–CHIT-rGO (0.01) membranes.

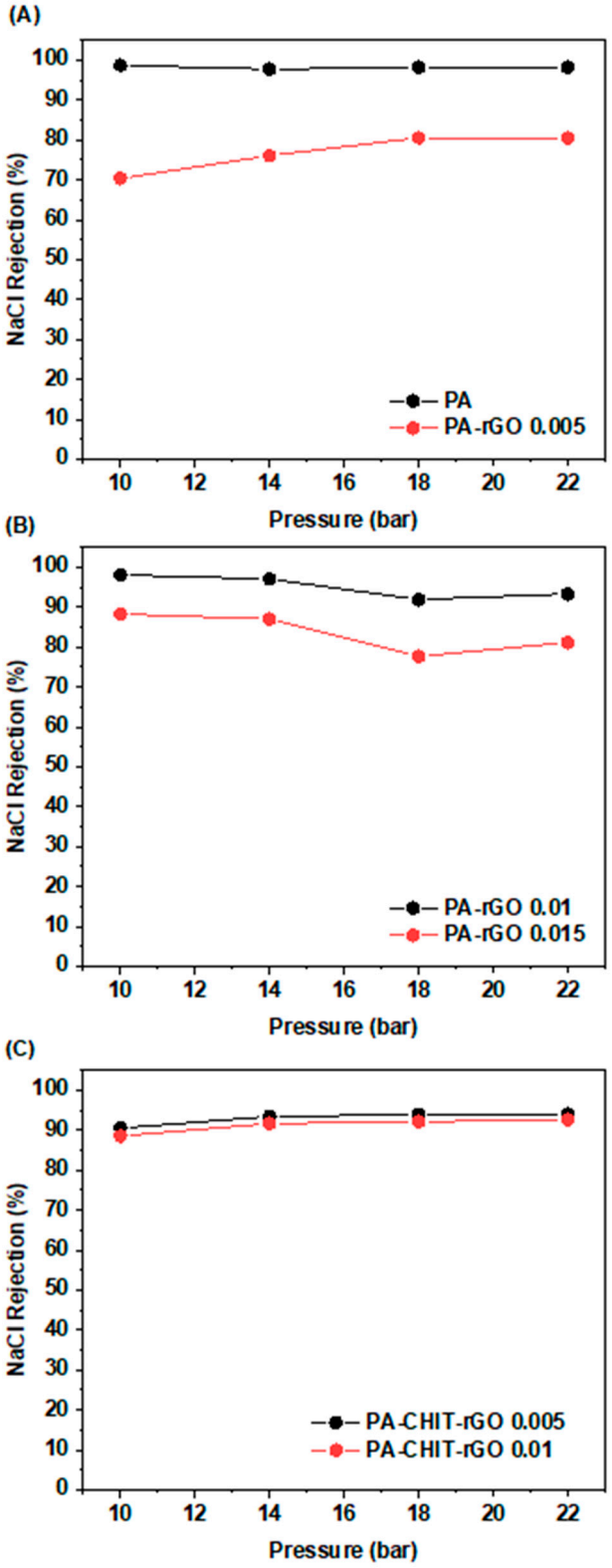

Figure 7. NaCl rejection of (**A**) PA and PA–rGO (0.005), (**B**) PA–rGO (0.01) and PA–rGO (0.015) and (**C**) PA–CHIT-rGO (0.005) and PA–CHIT-rGO (0.01) membranes.

Table 2. The evaluation of the composite membranes in previous reports, compared with the findings of this study.

Membranes	Water Flux ($L\ m^{-2}\ h^{-1}$) at 15 Bar	NaCl Salt Rejection % at 15 Bar	Ref.
PA	16.03	97.77	This work
PA–rGO (0.01%)	25.50	97.11	This work
PA–rGO (0.01)/CHIT	9.00	88.58	This work
PA–MWCNTs (0.1%)	15.45	96.76	[26]
PA–MWCNTs–COOH	36.225	96.43	[26]
PA–MWCNT–NH_2	27.75	97.11	[26]
PA–SiO_2 (1%)	47.9	98.9	[62]
NF	20	90	[63]
BWRO	20	>99	[63]
SWRO	20	>99	[63]

4. Conclusions

Explore the realm of advanced membrane technology! A focal point in recent research is the enhancement of the support layer in membrane methods, fine-tuning its surface to elevate performance to new heights. Unlike the usual polyimide, we opted for polyamide in our interfacial polymerization setup, playing with varying amounts of reduced graphene oxide (rGO). The result? Membranes that not only turbocharge water permeability but also ace salt rejection. While PA–rGO membranes lead to water permeability, PA–rGO/CHIT membranes steal the show, with 80–95% salt rejection prowess. Witness the future of membranes.

Author Contributions: Conceptualization, A.A.A. (Ahmed A. Alshahrani), A.A.E.-H. and I.H.A.; methodology, A.A.A. (Ahmed A. Alshahrani), A.A.E.-H. and I.H.A.; software, A.A.A. (Arwa A. Almutairi), D.A.A. and S.A.A.; validation, A.A.A. (Arwa A. Almutairi), D.A.A. and S.A.A.; formal analysis, A.A.A. (Arwa A. Almutairi), D.A.A. and S.A.A.; investigation, A.A.A. (Arwa A. Almutairi), D.A.A. and S.A.A.; resources, A.A.A. (Arwa A. Almutairi), D.A.A. and S.A.A.; data curation, A.A.A. (Arwa A. Almutairi), D.A.A. and S.A.A.; writing—original draft preparation, A.A.A. (Ahmed A. Alshahrani), H.M.A.H. and I.H.A.; writing—review and editing, A.A.A. (Ahmed A. Alshahrani), H.M.A.H. and I.H.A.; visualization, A.A.A. (Ahmed A. Alshahrani); supervision, A.A.A. (Ahmed A. Alshahrani), A.A.E.-H. and I.H.A.; project administration, A.A.A. (Ahmed A. Alshahrani), A.A.E.-H. and I.H.A.; funding acquisition, A.A.E.-H. All authors have read and agreed to the published version of the manuscript.

Funding: Princess Nourah Bint Abdulrahman University Researchers Supporting Project number (PNURSP2023R75), Princess Nourah Bint Abdulrahman University, Riyadh, Saudi Arabia.

Data Availability Statement: The data presented in this study are available in article.

Acknowledgments: Princess Nourah Bint Abdulrahman University Researchers Supporting Project number (PNURSP2023R75), Princess Nourah Bint Abdulrahman University, Riyadh, Saudi Arabia.

Conflicts of Interest: The authors declare no conflict of interest.

References

1. Shi, J.; Wu, W.; Xia, Y.; Li, Z.; Li, W. Confined interfacial polymerization of polyamide-graphene oxide composite membranes for water desalination. *Desalination* **2018**, *441*, 77–86. [CrossRef]
2. Werber, J.R.; Osuji, C.O.; Elimelech, M. Materials for next-generation desalination and water purification membranes. *Nat. Rev. Mater.* **2016**, *1*, 16018. [CrossRef]
3. Fane, A.G.; Wang, R.; Hu, M.X. Synthetic membranes for water purification: Status and future. *Angew. Chem. Int. Ed.* **2015**, *54*, 3368–3386. [CrossRef]
4. Abid, M.B.; Wahab, R.A.; Abdelsalam, M.; Gzara, L.; Moujdin, I.A. Desalination technologies, membrane distillation, and electrospinning, an overview. *Heliyon* **2023**, *9*, e12810. [CrossRef] [PubMed]
5. Koros, W.J.; Ma, Y.H.; Shimidzu, T. Terminology for membranes and membrane processes (IUPAC Recommendations 1996). *Pure Appl. Chem.* **1996**, *68*, 1479–1489. [CrossRef]

6. Kangwen, S. International Overview of Seawater Desalination Plant by Reverse Osmosis Technology. Master's Theses, Universitetet i Stavanger, Stavanger, Norway, 2012.
7. Mohammad, A.W.; Teow, Y.; Ang, W.; Chung, Y.; Oatley-Radcliffe, D.; Hilal, N. Nanofiltration membranes review: Recent advances and future prospects. *Desalination* **2015**, *356*, 226–254. [CrossRef]
8. Li, D.; Yan, Y.; Wang, H. Recent advances in polymer and polymer composite membranes for reverse and forward osmosis processes. *Prog. Polym. Sci.* **2016**, *61*, 104–155. [CrossRef]
9. Ghosh, A.K.; Jeong, B.-H.; Huang, X.; Hoek, E.M. Impacts of reaction and curing conditions on polyamide composite reverse osmosis membrane properties. *J. Membr. Sci.* **2008**, *311*, 34–45. [CrossRef]
10. Yin, J.; Zhu, G.; Deng, B. Graphene oxide (GO) enhanced polyamide (PA) thin-film nanocomposite (TFN) membrane for water purification. *Desalination* **2016**, *379*, 93–101. [CrossRef]
11. Yang, R.; Jang, H.; Stocker, R.; Gleason, K.K. Synergistic prevention of biofouling in seawater desalination by zwitterionic surfaces and low-level chlorination. *Adv. Mater.* **2014**, *26*, 1711–1718. [CrossRef]
12. Surawanvijit, S.; Rahardianto, A.; Cohen, Y. An Integrated approach for characterization of polyamide reverse osmosis membrane degradation due to exposure to free chlorine. *J. Membr. Sci.* **2016**, *510*, 164–173. [CrossRef]
13. Song, X.; Zhou, Q.; Zhang, T.; Xu, H.; Wang, Z. Pressure-assisted preparation of graphene oxide quantum dot-incorporated reverse osmosis membranes: Antifouling and chlorine resistance potentials. *J. Mater. Chem. A* **2016**, *4*, 16896–16905. [CrossRef]
14. Fathizadeh, M.; Tien, H.N.; Khivantsev, K.; Song, Z.; Zhou, F.; Yu, M. Polyamide/nitrogen-doped graphene oxide quantum dots (N-GOQD) thin film nanocomposite reverse osmosis membranes for high flux desalination. *Desalination* **2019**, *451*, 125–132. [CrossRef]
15. Yuan, H.; Ye, J.; Ye, C.; Yin, S.; Li, J.; Su, K.; Fang, G.; Wu, Y.; Zheng, Y.; Ge, M. Highly efficient preparation of graphite oxide without water enhanced oxidation. *Chem. Mater.* **2021**, *33*, 1731–1739. [CrossRef]
16. Abbaszadeh, M.; Krizak, D.; Kundu, S. Layer-by-layer assembly of graphene oxide nanoplatelets embedded desalination membranes with improved chlorine resistance. *Desalination* **2019**, *470*, 114116. [CrossRef]
17. Choi, W.; Choi, J.; Bang, J.; Lee, J.-H. Layer-by-layer assembly of graphene oxide nanosheets on polyamide membranes for durable reverse-osmosis applications. *ACS Appl. Mater. Interfaces* **2013**, *5*, 12510–12519. [CrossRef]
18. Tsou, C.-H.; An, Q.-F.; Lo, S.-C.; De Guzman, M.; Hung, W.-S.; Hu, C.-C.; Lee, K.-R.; Lai, J.-Y. Effect of microstructure of graphene oxide fabricated through different self-assembly techniques on 1-butanol dehydration. *J. Membr. Sci.* **2015**, *477*, 93–100. [CrossRef]
19. Kim, H.W.; Yoon, H.W.; Yoon, S.-M.; Yoo, B.M.; Ahn, B.K.; Cho, Y.H.; Shin, H.J.; Yang, H.; Paik, U.; Kwon, S. Selective gas transport through few-layered graphene and graphene oxide membranes. *Science* **2013**, *342*, 91–95. [CrossRef]
20. Romaniak, G.; Dybowski, K.; Jeziorna, A.; Kula, P.; Kaźmierczak, T. Synthesis and characterization of semi-permeable graphene/graphene oxide membranes for water desalination. *J. Mater. Sci.* **2020**, *55*, 9775–9786. [CrossRef]
21. Liu, Z.; Zhao, L.; Ye, H.; Wang, Z.; Chen, Y.; Li, Y.; Liu, L.; Guo, Y.; Chen, Y.; Niu, Q.J. Highly anions-selective polyamide nanofiltration membrane fabricated by rod-coating assisted interfacial polymerization. *J. Membr. Sci.* **2023**, *668*, 121273. [CrossRef]
22. Abu-Dalo, M.A.; Bozeya, A.; Sawalmeh, Z.; Albiss, B.; Alnairat, N.; Abu-Zurayk, R. Antifouling polymeric nanocomposite membrane based on interfacial polymerization of polyamide enhanced with green TiO_2 nanoparticles for water desalination. *PeerJ Anal. Chem.* **2023**, *5*, 26. [CrossRef]
23. Fathizadeh, M.; Aroujalian, A.; Raisi, A. Effect of added NaX nano-zeolite into polyamide as a top thin layer of membrane on water flux and salt rejection in a reverse osmosis process. *J. Membr. Sci.* **2011**, *375*, 88–95. [CrossRef]
24. Junior, F.L.F. *Application of Graphene Oxide and Reduced Graphene Oxide in Desalination Membranes*; PUC-Rio: Rio de Janeiro, Brazil, 2022.
25. Fajardo-Diaz, J.; Takeuchi, K.; Morelos-Gomez, A.; Cruz-Silva, R.; Yamanaka, A.; Tejima, S.; Izu, K.; Saito, S.; Ito, I.; Maeda, J. Enhancing boron rejection in low-pressure reverse osmosis systems using a cellulose fiber–carbon nanotube nanocomposite polyamide membrane: A study on chemical structure and surface morphology. *J. Membr. Sci.* **2023**, *679*, 121691. [CrossRef]
26. Alterary, S.S.; Alyabes, R.M.; Alshahrani, A.A.; Al-Alshaikh, M.A. Unfunctionalized and Functionalized Multiwalled Carbon Nanotubes/Polyamide Nanocomposites as Selective-Layer Polysulfone Membranes. *Polymers* **2022**, *14*, 1544. [CrossRef]
27. Li, J.; Cheng, L.; Song, W.; Xu, Y.; Liu, F.; Wang, Z. In-situ sol-gel generation of SiO_2 nanoparticles inside polyamide membrane for enhanced nanofiltration. *Desalination* **2022**, *540*, 115981. [CrossRef]
28. Zhan, X.; Zhang, G.; Chen, X.; He, R.; Zhang, Q.; Chen, F. Improvement of antifouling and antibacterial properties of poly (ether sulfone) UF membrane by blending with a multifunctional comb copolymer. *Ind. Eng. Chem. Res.* **2015**, *54*, 11312–11318. [CrossRef]
29. Mansourpanah, Y.; Ghanbari, A.; Yazdani, H.; Mohammadi, A.G.; Rahimpour, A. Silver-polyamidoamine/graphene oxide thin film nanofiltration membrane with improved antifouling and antibacterial properties for water purification and desalination. *Desalination* **2021**, *511*, 115109. [CrossRef]
30. Alkhouzaam, A.; Qiblawey, H. Synergetic effects of dodecylamine-functionalized graphene oxide nanoparticles on antifouling and antibacterial properties of polysulfone ultrafiltration membranes. *J. Water Process Eng.* **2021**, *42*, 102120. [CrossRef]
31. Chae, H.-R.; Lee, J.; Lee, C.-H.; Kim, I.-C.; Park, P.-K. Graphene oxide-embedded thin-film composite reverse osmosis membrane with high flux, anti-biofouling, and chlorine resistance. *J. Membr. Sci.* **2015**, *483*, 128–135. [CrossRef]
32. Kim, S.G.; Hyeon, D.H.; Chun, J.H.; Chun, B.-H.; Kim, S.H. Novel thin nanocomposite RO membranes for chlorine resistance. *Desalination Water Treat.* **2013**, *51*, 6338–6345. [CrossRef]

33. Ali, M.E.; Wang, L.; Wang, X.; Feng, X. Thin film composite membranes embedded with graphene oxide for water desalination. *Desalination* **2016**, *386*, 67–76. [CrossRef]
34. Chae, H.-R.; Lee, C.-H.; Park, P.-K.; Kim, I.-C.; Kim, J.-H. Synergetic effect of graphene oxide nanosheets embedded in the active and support layers on the performance of thin-film composite membranes. *J. Membr. Sci.* **2017**, *525*, 99–106. [CrossRef]
35. Kim, H.; Ahn, D.; Annable, M.D. Enhanced removal of VOCs from aquifers during air sparging using thickeners and surfactants: Bench-scale experiments. *J. Contam. Hydrol.* **2016**, *184*, 25–34. [CrossRef] [PubMed]
36. Castarlenas, S.; Téllez, C.; Coronas, J. Gas separation with mixed matrix membranes obtained from MOF UiO-66-graphite oxide hybrids. *J. Membr. Sci.* **2017**, *526*, 205–211. [CrossRef]
37. Doğu, M.; Ercan, N. High performance cyclic olefin copolymer (COC) membranes prepared with melt processing method and using of surface modified graphitic nano-sheets for H_2/CH_4 and H_2/CO_2 separation. *Chem. Eng. Res. Des.* **2016**, *109*, 455–463. [CrossRef]
38. Zahirifar, J.; Karimi-Sabet, J.; Moosavian, S.M.A.; Hadi, A.; Khadiv-Parsi, P. Fabrication of a novel octadecylamine functionalized graphene oxide/PVDF dual-layer flat sheet membrane for desalination via air gap membrane distillation. *Desalination* **2018**, *428*, 227–239. [CrossRef]
39. Wang, J.; Wang, Y.; Zhang, Y.; Uliana, A.; Zhu, J.; Liu, J.; Van der Bruggen, B. Zeolitic imidazolate framework/graphene oxide hybrid nanosheets functionalized thin film nanocomposite membrane for enhanced antimicrobial performance. *ACS Appl. Mater. Interfaces* **2016**, *8*, 25508–25519. [CrossRef]
40. Ma, W.; Chen, T.; Nanni, S.; Yang, L.; Ye, Z.; Rahaman, M.S. Zwitterion-functionalized graphene oxide incorporated polyamide membranes with improved antifouling properties. *Langmuir* **2018**, *35*, 1513–1525. [CrossRef]
41. Xue, S.-M.; Ji, C.-H.; Xu, Z.-L.; Tang, Y.-J.; Li, R.-H. Chlorine resistant TFN nanofiltration membrane incorporated with octadecylamine-grafted GO and fluorine-containing monomer. *J. Membr. Sci.* **2018**, *545*, 185–195. [CrossRef]
42. Alberto, M.; Bhavsar, R.; Luque-Alled, J.M.; Prestat, E.; Gao, L.; Budd, P.M.; Vijayaraghavan, A.; Szekely, G.; Holmes, S.M.; Gorgojo, P. Study on the formation of thin film nanocomposite (TFN) membranes of polymers of intrinsic microporosity and graphene-like fillers: Effect of lateral flake size and chemical functionalization. *J. Membr. Sci.* **2018**, *565*, 390–401. [CrossRef]
43. Li, W.; Zhang, Y.; Xu, Z.; Yang, A.; Meng, Q.; Zhang, G. Self-assembled graphene oxide microcapsules with adjustable permeability and yolk–shell superstructures derived from atomized droplets. *Chem. Commun.* **2014**, *50*, 15867–15869. [CrossRef] [PubMed]
44. Li, W.; Zhang, Y.; Su, P.; Xu, Z.; Zhang, G.; Shen, C.; Meng, Q. Metal–organic framework channelled graphene composite membranes for H 2/CO 2 separation. *J. Mater. Chem. A* **2016**, *4*, 18747–18752. [CrossRef]
45. Hung, W.-S.; Tsou, C.-H.; De Guzman, M.; An, Q.-F.; Liu, Y.-L.; Zhang, Y.-M.; Hu, C.-C.; Lee, K.-R.; Lai, J.-Y. Cross-linking with diamine monomers to prepare composite graphene oxide-framework membranes with varying d-spacing. *Chem. Mater.* **2014**, *26*, 2983–2990. [CrossRef]
46. Han, Y.; Xu, Z.; Gao, C. Ultrathin graphene nanofiltration membrane for water purification. *Adv. Funct. Mater.* **2013**, *23*, 3693–3700. [CrossRef]
47. Echaide-Górriz, C.; Sorribas, S.; Téllez, C.; Coronas, J. MOF nanoparticles of MIL-68 (Al), MIL-101 (Cr) and ZIF-11 for thin film nanocomposite organic solvent nanofiltration membranes. *RSC Adv.* **2016**, *6*, 90417–90426. [CrossRef]
48. Sorribas, S.; Gorgojo, P.; Téllez, C.; Coronas, J.; Livingston, A.G. High flux thin film nanocomposite membranes based on metal–organic frameworks for organic solvent nanofiltration. *J. Am. Chem. Soc.* **2013**, *135*, 15201–15208. [CrossRef] [PubMed]
49. Jeong, B.-H.; Hoek, E.M.; Yan, Y.; Subramani, A.; Huang, X.; Hurwitz, G.; Ghosh, A.K.; Jawor, A. Interfacial polymerization of thin film nanocomposites: A new concept for reverse osmosis membranes. *J. Membr. Sci.* **2007**, *294*, 1–7. [CrossRef]
50. Lind, M.L.; Ghosh, A.K.; Jawor, A.; Huang, X.; Hou, W.; Yang, Y.; Hoek, E.M. Influence of zeolite crystal size on zeolite-polyamide thin film nanocomposite membranes. *Langmuir* **2009**, *25*, 10139–10145. [CrossRef]
51. Arsuaga, J.M.; Sotto, A.; del Rosario, G.; Martínez, A.; Molina, S.; Teli, S.B.; de Abajo, J. Influence of the type, size, and distribution of metal oxide particles on the properties of nanocomposite ultrafiltration membranes. *J. Membr. Sci.* **2013**, *428*, 131–141. [CrossRef]
52. Goh, P.; Ismail, A.; Ng, B. Carbon nanotubes for desalination: Performance evaluation and current hurdles. *Desalination* **2013**, *308*, 2–14. [CrossRef]
53. Abolhassani, M.; Griggs, C.S.; Gurtowski, L.A.; Mattei-Sosa, J.A.; Nevins, M.; Medina, V.F.; Morgan, T.A.; Greenlee, L.F. Scalable chitosan-graphene oxide membranes: The effect of GO size on properties and cross-flow filtration performance. *ACS Omega* **2017**, *2*, 8751–8759. [CrossRef] [PubMed]
54. Deng, H.; Sun, P.; Zhang, Y.; Zhu, H. Reverse osmosis desalination of chitosan cross-linked graphene oxide/titania hybrid lamellar membranes. *Nanotechnology* **2016**, *27*, 274002. [CrossRef] [PubMed]
55. Gupta, S.; Evans, B. Interplay of graphene oxide and interfacial polymerized polyamide-crosslinked thin-film composite membranes for enhanced performance during reverse osmosis. *Desalin. Water Treat* **2021**, *218*, 177–192. [CrossRef]
56. Ren, X.; Ji, D.; Wen, X.; Bustamante, H.; Daiyan, R.; Foller, T.; Khine, Y.Y.; Joshi, R. Graphene oxide membranes for effective removal of humic acid. *J. Mater. Res.* **2022**, *37*, 3362–3371. [CrossRef]
57. Singh, K.; Devi, S.; Bajaj, H.; Ingole, P.; Choudhari, J.; Bhrambhatt, H. Optical resolution of racemic mixtures of amino acids through nanofiltration membrane process. *Sep. Sci. Technol.* **2014**, *49*, 2630–2641. [CrossRef]
58. Kovalchuk, A.; Huang, K.; Xiang, C.; Martí, A.A.; Tour, J.M. Luminescent polymer composite films containing coal-derived graphene quantum dots. *ACS Appl. Mater. Interfaces* **2015**, *7*, 26063–26068. [CrossRef]

59. Alawady, A.R.; Alshahrani, A.A.; Aouak, T.A.; Alandis, N.M. Polysulfone membranes with CNTs/Chitosan biopolymer nanocomposite as selective layer for remarkable heavy metal ions rejection capacity. *Chem. Eng. J.* **2020**, *388*, 124267. [CrossRef]
60. Nie, L.; Goh, K.; Wang, Y.; Lee, J.; Huang, Y.; Karahan, H.E.; Zhou, K.; Guiver, M.D.; Bae, T.-H. Realizing small-flake graphene oxide membranes for ultrafast size-dependent organic solvent nanofiltration. *Sci. Adv.* **2020**, *6*, eaaz9184. [CrossRef]
61. Shao, F.; Dong, L.; Dong, H.; Zhang, Q.; Zhao, M.; Yu, L.; Pang, B.; Chen, Y. Graphene oxide modified polyamide reverse osmosis membranes with enhanced chlorine resistance. *J. Membr. Sci.* **2017**, *525*, 9–17. [CrossRef]
62. Yan, W.; Wang, Z.; Wu, J.; Zhao, S.; Wang, J.; Wang, S. Enhancing the flux of brackish water TFC RO membrane by improving support surface porosity via a secondary pore-forming method. *J. Membr. Sci.* **2016**, *498*, 227–241. [CrossRef]
63. Yang, Z.; Guo, H.; Tang, C.Y. The upper bound of thin-film composite (TFC) polyamide membranes for desalination. *J. Membr. Sci.* **2019**, *590*, 117297. [CrossRef]